Parametric study of low-profile vortex generators

P. Martı´nez-Filgueira [a], *U. Fernandez-Gamiz* [a,*], *E. Zulueta* [b], *I. Errasti* [a], *B. Fernandez-Gauna* [c]

[a] *University of the Basque Country, UPV/EHU, Nuclear Engineering & Fluid Mechanics Department, Nieves Cano 12, 01016, Vitoria-Gasteiz, Spain*

[b] *University of the Basque Country, UPV/EHU, System Engineering & Automation Control Department, Nieves Cano 12, 01016, Vitoria-Gasteiz, Spain*

[c] *University of the Basque Country, UPV/EHU, Computational Intelligence Group, Nieves Cano 12, 01016, Vitoria-Gasteiz, Spain*

a b s t r a c t

Vortex generators (VGs) are flow control devices employed to avoid or delay flow separa- tion. In most cases, the VG is calculated with the same height as the boundary layer (BL) thickness at the device position. However, these so-called conventional VGs may produce overload drag in some applications. The low-profile VGs can decrease the residual drag linked to this kind of passive flow control actuators. The main goal of the present work is to investigate the trajectory and size of the primary vortex produced by low-profile VGs on a flat plate with a height to length ratio of ½ and a vane incident angle of 18.5º. Hence, nu- merical simulations have been performed using NaviereStokes equations at *Re* ¼ 1350 based on the local boundary layer thickness where the VG was placed. Additionally, a prediction model has been developed to describe the progression of the vortex size behind the passive vanes.

Introduction

Wind Energy nowadays contributes to the mitigation of the climate change avoiding emissions of hundreds of tons of carbon dioxide to the atmosphere. According to the European Wind Energy Association, wind energy has around a 15% share of the total European power capacity. The growth of installed wind power, a yearly 9% in Europe for the last fifteen years, along with the

growing importance of offshore wind energy shows the relevance of research in the discipline of flow control to maximize the energy output [1]. The wind related industry is generating thousands of jobs worldwide and the costs of this technology are expected to keep on declining in the coming years and onshore wind is the cheapest form of new power generation in Europe. Addition- ally, offshore wind will probably play a key role in Europe's power generation. Some energy researchers studied and quantified the penetration of global onshore wind energy in the next future as for instance Dai et al. [2]. In 2030, wind is expected to serve around 25% of the European electricity needs.

Nowadays, the increasingly complexity and size of the wind turbines is a widespread trend in the wind industry and a better comprehension of the aerodynamics to design effi- cient operational turbines is needed. The interactions of flow phenomena such as wake or atmospheric boundary layer effects in these new large wind turbines have to be modeled and simulated. Thus, G. Espan-a et al. [3] studied the wake behavior of a modeled wind turbine when large scale turbu- lent eddies are involved. Realistic simulations reproducing these flow interactions and appropriate methods of verifica- tion with will allow the design of efficient and state-of-the-art wind turbines. Technical aspects such as turbine perfor- mance, loading during extreme weather, component lifetime, noise generation or power output optimization are also key points to be analysed and further research has to be carried out. Thus, Kim et al. [4] studied the wake influence on the wind characteristics and fatigue mechanical loads in turbines. Kahla et al. [5] employed an algorithm based on particle swarm optimization in order to control the turbine's rotor side converter. Additionally, the design of control systems using the wind flow condition or algorithms to enhance the wind turbine stability are also needed. Dahbi et al. [6] developed a pitch angle control system of a variable-speed wind turbine using permanent magnet synchronous generator (PMSG) connected to the grid by means of fully controlled frequency converters to maximize the exploited wind power and to benefit from a wide range of the wind speed.

Flow separation control and the energy losses associated with the boundary layer have emerged as a key point in certain industrial fluid dynamics applications. Furthermore, the deficit of momentum in the boundary layer plays a major role in flow separation. The flow detachment from a contin- uous surface is governed by the adverse pressure gradient and the viscosity. If the flow must remain attached to the wall, the stream should have enough energy to overcome the adverse pressure gradient, the viscous dissipation along the flow path and the energy loss caused by the modification in momentum. This loss in energy is more prominent in the neighborhood

of the surface where the momentum and energy are much less than in the most distant part of the shear layer. Therefore, if the loss is such that further advancement of the fluid is no longer possible, then the flow separates from the surface.

Vortex generators (VGs) are passive devices to control flow which are able to change the motion performance of the fluid in the boundary layer region. VGs are small vanes not aligned with the incoming flow and located neighboring the leading edge. They act by exchanging momentum from the distant flow region to the wall-closed inner region. Researchers have applied these devices in certain aerodynamics applications in the past fifty years.

In Fig. 1a and b, two pairs of rectangular and triangular vortex generators (VGs) of the most-often type used in

different aerodynamics applications are shown. The customary VG height is usually similar to the local boundary layer thickness with a 1:2 height to length ratio. These devices modify the flow streamline direction creating flow vorticity. Thus, they generate downstream co-rotating or counter- rotating vortices depending on their geometrical configuration.

The installation of these vortex generators mounted on the suction side of aircraft wings or wind turbine blades may be considered a first approach to try to regulate the flow sepa- ration because they are easy to design and set-up as well as inexpensive. They can be quite easily assembled as a post- production fix to the wing or blade when the latter does not work as efficiently as expected. They are also replaceable by a simple and fast procedure and because of their small size a relatively big number of them are able to be spanwise distributed. On the other hand, active devices need an addi- tional energy source to get the desired effect on the flow and, unlike VGs and other passive devices, active flow control needs complex algorithms to get the maximum benefit [7].

These passive flow control devices are used to augment mixing in both free-shear and wall-bounded flows by expanding the active area where the energy transport occurs, setting off possible flow instabilities, accelerating laminar to turbulent transition and intensifying the turbulence once the shear flow becomes turbulent. Vortex generators also allow the formation of auxiliary flows as a way to successfully improving blending in laminar and turbulent flows. In other cases where flow mixing is involved, like heat exchangers, turbulence generating dimpled surfaces enhance heat trans- fer drawing on the strengths of turbulent boundary layer properties [8].

On the other hand, VGs generate a small parasitic drag and they need a detailed understanding to be applied correctly and optimized for every flow and geometry. In the work carried by Gao et al. [9] on a 30% thick DU97-W-300 airfoil, the maximum lift coefficient was substantially

increased with the insertion of passive VGs. This effect is the result from the delay or prevention of the boundary layer detachment, however, this good performance was counterbalanced by the appearance of a considerable parasitic drag.

Inflow turbulence, gusts and yaw misalignment cause dy- namic stall in wind turbine blades. This process takes place with sudden increases of the angle of attack and both lift and drag coefficients rise up to values greater than the ones reached in steady state conditions. A vortex structure grows and once it's shed, the airfoil goes into deep stall state, where

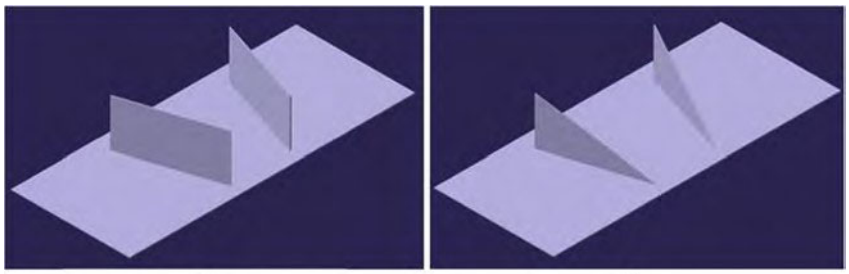

Fig. 1 Sketch of a pair of (a) rectangular (left side) and (b) triangular (right side) counter-rotating VGs.

loss of lift is bigger than in steady operation [10]. The non- linear and unsteady aerodynamic behavior of large horizontal-axis wind turbines is a problem from the structural and electric generation point of view. The employment of VGs can lead to a reduction of periodic loads thus improving power output and cyclic fatigue life [11].

In the past years, some models focusing on the vortices produced by vanes have been implemented. For instance, Smith [12] proposed a theoretical model as well as Velte et al. [13] who showed the helical symmetry of vortices produced by a passive four-sided vane-type vortex generator. Additionally, there are VG models using the BAY-model [14] which have been implemented into codes as the Actuator VG model (AcVG) developed in Ref. [15]. These authors introduced body forces by means of source expressions in the energy and momentum equations to reproduce the existence of a passive flow control device.

Triangular and rectangular conventional VGs have been implemented onto wings of airplanes for flow control to effi- ciently improve mixing of the boundary layer and transfer momentum nearby the wall by delaying or suppressing the flow detachment [16]. Furthermore, in the experimental work performed by Velte [17] and the associated simulations carried out by Fernandez-Gamiz et al. [18] demonstrated that the primary vortex produced by a rectangular VG inserted on a flat plate exhibited self-similarity for axial and azimuthal veloc- ities. In most applications, these VG devices are designed with their height h similar to the local boundary layer

thickness d and inserted perpendicular to the surface with an incident angle to the flow to produce streamwise vortices. However, the remaining drag related to these d-*scale* VG devices might be relatively large in some flow-control application.

The generation of streamwise vortices by means of the insertion of vane-type devices with reduced height is an easy method to enhance their efficiency. Lin et al. [19] proved that when decreasing the height of standard VGs to a value lower than the local boundary layer thickness, the momentum transfer keeps being large enough to avoid or delay flow sep- aration downstream of the VGs. These so-called low-profile VGs were mounted on multi-element high-lift airfoils with the aim of controlling the flow detachment on the flap. Yao et al.
[20] compared the deviation in the vortex path between a low- profile VG with height *h* around 20% the boundary layer thickness d and a standard VG with height *h* around 20% the boundary layer thickness d and a conventional VG with *h* ¼ d.

Ashill et al. [21] in an conceptual and experimental study showed a successful delay of the shock-induced separation on a transonic profile by mounting Sub Boundary Layer Vortex Generators (SBVG). Those wedge SBVGs proved to produce meaningful rises in lift and diminutions in drag. According to [22], the implementation of these low-profile VG devices could be considered as a quite good option to be implemented when the flow-separation positions are relatively fixed and the vanes can be implemented upstream relatively nearly the flow separation.

The main objective of this study is to analyze the size and path of the primary vortex produced by a four-sided low- profile (sub d-*scale*) VG implemented on a flat plate with negligible streamwise pressure gradient for five vane heights h ¼ d, h_1 ¼ 0.8d, h_2 ¼ 0.6d, h_3 ¼ 0.4d and h_4 ¼ 0.2d where d is the local boundary layer thickness and h_i represents the VG height for each case (see Fig. 2). StarCCMþ® CFD code provided by CD- Adapco was run for the computations applying the Reynolds- Average NaviereStokes (RANS) method at Reynolds number Re_d ¼ 1350 computed taking into account the boundary layer thickness of d ¼ 0.25 m at the VG position.

The studied cases consist of a single vortex generator VG implemented on a flat plate with an angle of attack with respect to the flow of b ¼ 18.5º. Previously, the flow generated over the same flat plate with the VG removed was also simulated to estimate the boundary layer thickness d at the VG mounted position. This work is a contribution to a better comprehension of the performance of the primary vortex downstream of the so-called low-profile vortex generators VGs and consequently, a contribution to be able to exploit the main advantages of these vanes, such as their simplicity, non expensive implementation and small drag.

Numerical setup

In the current work, the numerical solution has been reached applying RANS equations for steady state flow in a finite vol- ume flow solver for structured grids. QUICK scheme [23] is used to discretize the convective terms ensuring the robust- ness of the solution. The turbulence is modeled through the *k* e u *SST* turbulence model by Menter [24]. Steady state com- putations have been successfully applied to a single VG case placed on a flat plate at two different angles of attack with respect to the oncoming flow [25]. The comparison of the flow

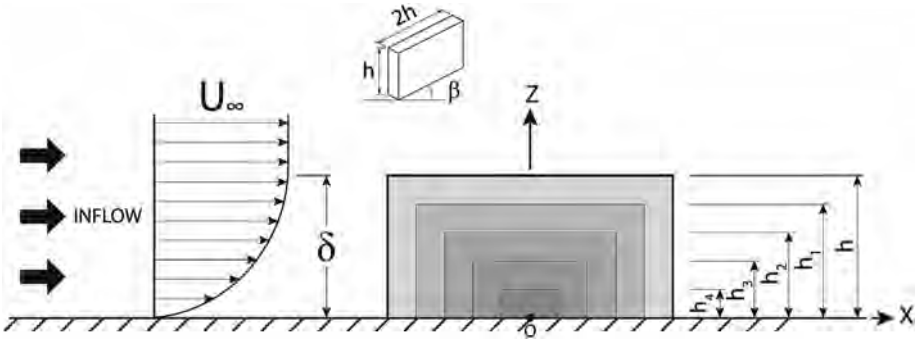

Fig. 2 VG dimensions with constant height to length ratio 1:2.

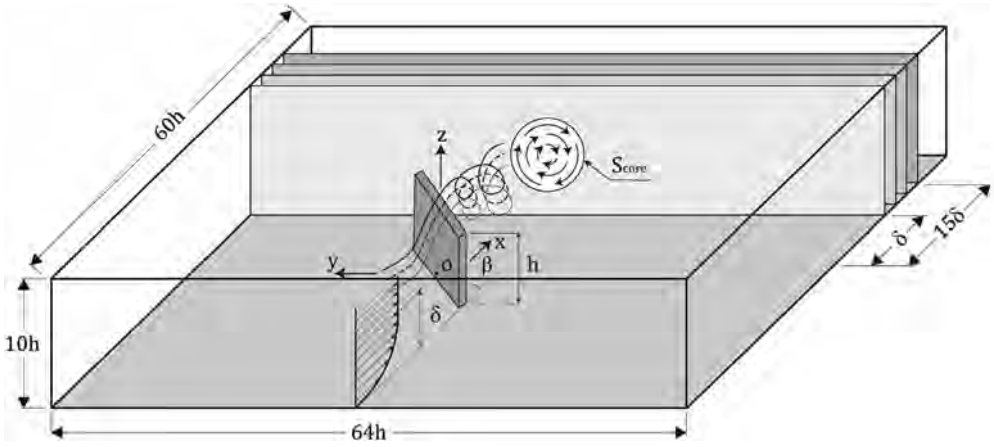

Fig. 3 Computational domain (not to scale).

field with experimental results achieved good agreement with the exception of the near wake downstream the vane.

The computational setup can be seen on Fig. 3. The size of the fluid region is normalized with the conventional VG height *h*, and its measurements are represented in Fig. 3. At the bottom wall and on the VG surface, no-slip conditions were specified, while the upstream and lid part of the domain were specified as inflow conditions with prescribed velocity ac- cording to the undisturbed velocity. The two side faces of the domain were specified as slip/symmetry conditions, while the downstream plane was set as an outlet assuming a fully developed flow. At the inlet, the turbulence is set to give low eddy viscosity, and the turbulence seen by the VG is generated by the developing boundary layer along the wall surface.

The vortex generator is a vane with constant thickness, and is positioned normal to the plate at a point far enough from the velocity inlet to allow the boundary layer thickness to equal the height of the conventional VG, d ¼ *h*. The shape of the vane is rectangular and its height to length ratio is kept constant to a 1:2 value for all cases, Fig. 2. The boundary layer thickness at the VG position is 0.25 m.

In this research, the angle of attack of the vortex generator to the oncoming flow is b ¼ 18.5º and the Reynolds number is *Re* ¼ 1350 based on the inflow velocity U_∞ ¼ 1 ms^{-1}, the density of the fluid 1 kg m^{-3}, and the local boundary layer thickness as the reference length, d ¼ 0.25 m. The angle of attack of the vane is close to the optimum one found by Stanislas and Godard [26] in a flow control optimization parametric study. A 20 million cell block structured grid conforms the computa- tional domain, with a height D*z/h* ¼ 1.5 x 10^{-5} for the cells surrounding the walls. This way, the turbulence model mesh resolution needs are provided, with a dimensionless distance less than 1 ($y^þ < 1$) in any wall. In the proximity of the vane, the mesh contains 6.5 x 10^6 cells, and the mesh downstream of the vortex generator created for a proper capturing of the wake has about 11.5 x 10^6 cells, as shown in Fig. 4. The hy- perbolic tangent stretching function of [27] was used as grid stretching method.

The vortex center location and velocity components were extracted in 15 spanwise planes from the simulation, normal to the main flow direction and to the plate and placed from 1 to 15 times the boundary layer thickness downstream of the VG, Fig. 3.

Results

A mesh resolution study has been carried out on the standard VG case to verify enough grid resolution. Fig. 5 summarizes the results obtained for the finer mesh level 1 which are compared with results obtained for a standard level 2 and a coarser mesh level 3. This figure represents the axial u_x and azimuthal u_q velocity profiles for three grid levels. The previ- ous velocity profiles were calculated on a line parallel to the

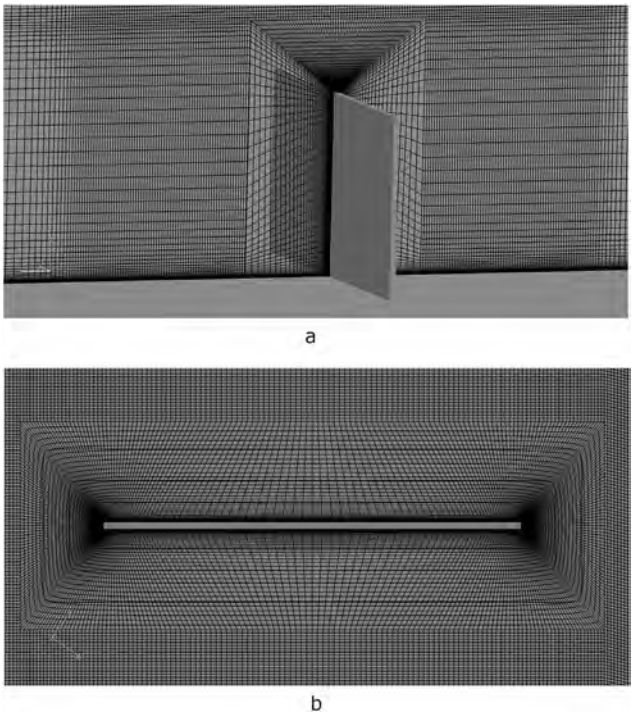

Fig. 4 Mesh sections on the VG position. (a) cross-flow section. (b) top view.

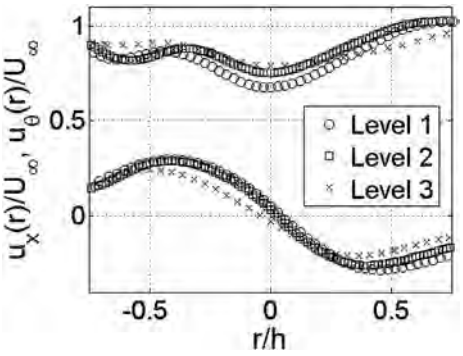

Fig. 5 Axial u_x and azimuthal u_q velocity profiles for three different mesh sizes of the computations.

plate and passing through the core center of the primary vortex. The line was located in a plane perpendicular to the streamwise direction positioned at five conventional vane heights behind the VG. Less than 5% of mesh dependency was detected for both axial and azimuthal velocities. The mesh level 1 was used for all the computations of the current study. The iterative solution process was carried out until the re- sidual error drops below 10^{-5} for velocities, pressure and turbulence quantities.

The vortex generated by a single passive VG on a flat plate was modeled by numerical simulations. Four different low- profile vanes were chosen in the present study: h_1 ¼ 0.8d, h_2 ¼ 0.6d, h_3 ¼ 0.4d and h_4 ¼ 0.2d, at b ¼ 18.5º were used and their results compared with those of the conventional VG h ¼ d. The data were extracted from the numerical simulations with an analogous procedure of the study of [18]. The three velocity components were extracted along lines crossing the center of the primary vortex in planes at 5d, 10d and 15d normal to the wall and also normal to the streamwise direc- tion capture the growth of the longitudinal vortex. The cy- lindrical coordinate system used to describe these variations across the vortex core is also presented in Ref. [18], with the origin at all times placed at the center of the vortex.

The solid lines of Fig. 6 represent the axial u_x and azimuthal u_q velocity profiles of the analytical model of Velte [17]. This analytical model is based on the Batchelor vortex model [28], which includes the non uniform axial velocity distribution u_x which approaches the LambeOseen vortex in the extreme. Flows with helical vorticity can be described by means of the correlation between the axial and circumferential vorticity vector components. According to Velte [17], the Batchelor vortex model is chosen as described in Equation (1):

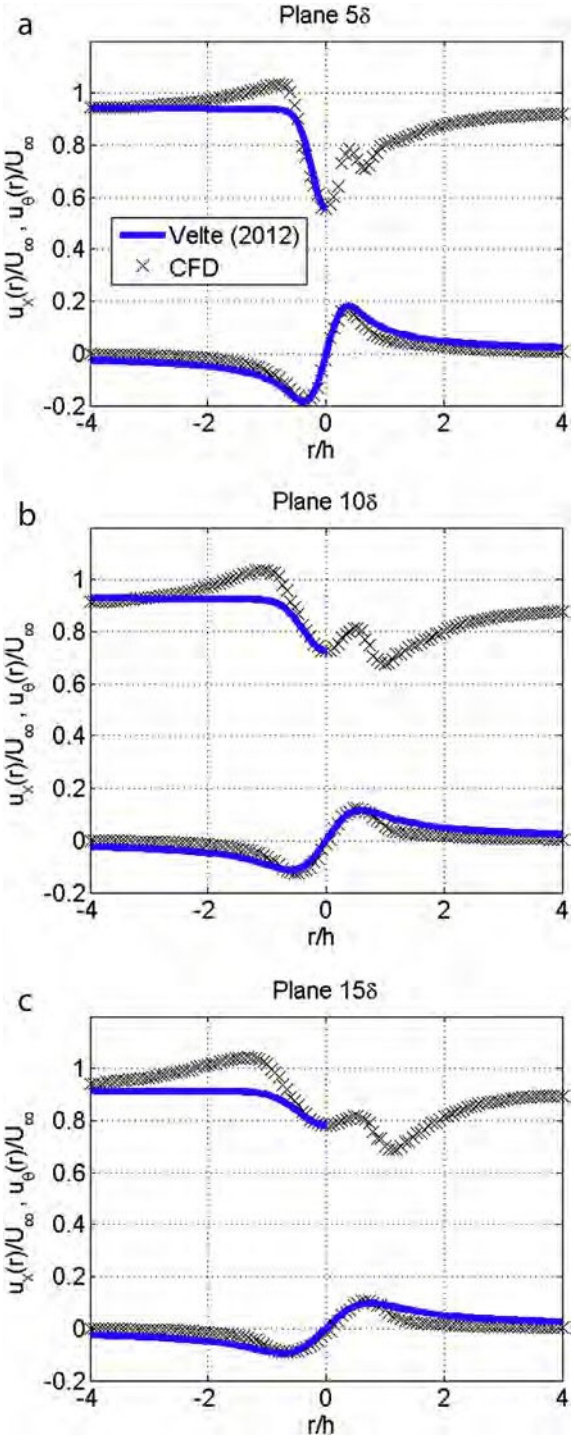

Fig. 6 Axial u_x (upper part) and azimuthal u_q (lower part) velocity profiles produced by a rectangular VG with an

$u_q ¼ \frac{G}{2pr} 1 - \exp$

profiłes by solid lines.

$u_x ¼ u_0 - \frac{}{2pl} 1 - \exp \varepsilon 2$

The only requirements of this simple model are the size of the vortex core defined by the vortex radius ε, the circulation G, the helical pitch l and the vortex convection velocity u_0. r is the distance calculated from the origin located in the vortex center and parallel to the wall.

The axial and azimuthal velocity profiles defined by Equation (1) were compared with the computational profiles corresponding to the conventional VG h. Note that the com- parison has been carried out only on the left side, due to a

perturbing secondary vortex appearing on the right side yielding an asymmetric velocity profile [13]. The analytical model overlaps quite well the computational azimuthal ve- locity profiles and is able to reproduce the vortex convection velocity. Nevertheless, some differences are evident in the axial velocity. Due to the interaction with the wall and the perturbation of the secondary vortex, the axial velocity profile of the computations reaches higher values than the non per- turbed velocity of U_∞ ¼ 1 m s^{-1} which is not well reproduced by the analytical model.

According to [25] and [17], up to three parameters were identified to characterize the streamwise vortices evolution downstream of vane-type VGs: the peak vorticity, the trajec- tory and the size of the vortex. The center of the vortex is determined by calculating the peak vorticity at every plane behind the trailing edge of the VG and, as a result, the path of the vortex. Moreover, the circulation is another factor asso- ciated to the vortex induced rate of mixing of the outer part of the flow with the BL [29]. The trajectory of the primary vortex produced by passive VGs also plays a decisive task in the mixing performance.

Trajectory of the streamwise vortex

The vertical z and lateral y trajectory of the vortex were determined by calculating the position of the center of the vortex on the downstream axis x. Fig. 7 shows a comparison between the paths followed by the vortex generated by the conventional VG h and the vortices generated by the low- profile VGs h_1, h_2, h_3 and h_4. Both lateral and vertical co- ordinates and streamwise coordinates are normalized by the local boundary layer thickness d corresponding to the con- ventional VG h to illustrate the influence of VG scaling on the wake of the passive vanes.

The lateral trajectories of the standard VG h and the lower profile VGs h_1, h_2, h_3 have a similar tendency, see Fig. 7a. However, for the lowest VG h_4, the lateral trajectory is nearly parallel to the streamwise direction behind the VG and achieving the minimum deviation in the y direction in com- parison with the other cases with larger vane size. Immedi- ately behind the trailing

edge of the VGs, the vortex trajectories of all cases initiate from approximately the same position in spite of the vane height.

The vortex trajectories of every case have been represented in Fig. 7b for the vertical direction. The trajectory of the vortex in the vertical direction decreases proportionally as the vane size decreases and remains approximately within the order of the consequent VG height with the exception of the lowest vane h_4, which behaves in a different way. In this case the slope of the vertical path is much higher than all the other cases, thus the elevation of the vortex center is quite large in comparison with the other cases at locations far away from the passive device.

It is remarkable that the location of the vortex center stays within the boundary layer and remains roughly parallel to the wall with the exception of the smallest vane h_4. As a reference, Fig. 7b also shows the relative height of the BL for the baseline flat plate flow without a VG device. The solid line represents the baseline BL thickness which varies from z/d ¼ 1 at the VG location to z/d ¼ 1.27 at the farthest downstream position of 15d.

The non-dimensional vortex trajectories for all the low- profile VGs follow the same tendency for both lateral and vertical directions in comparison with the standard VG h, except for the lowest device h_4. In this case, the gradient of the vertical path is larger than the other cases, mainly for loca- tions far away from the VG. Therefore, due to the low size of the vane, the vortex generated by the VG h_4 is quite close to the viscous sublayer where the viscous (molecular) shear is pre- vailing, in consequence there is powerful interaction with the wall.

Vortex decay

Additionally to the previously mentioned results on the lateral and the vertical trajectories of the vortex, the largest value of the streamwise vorticity has also been investigated. To show the vortex decay, the streamwise distribution of the normal- ized peak vorticity ($u_{x,max}$ d)/U_∞ is plotted as a function of the non-dimensional downstream distance x/d for all cases stud- ied. The vortex decay is represented in Fig. 8a in the down- stream direction and proves that the peak vorticity is quickly mitigated downstream of the trailing edge of the VG for all

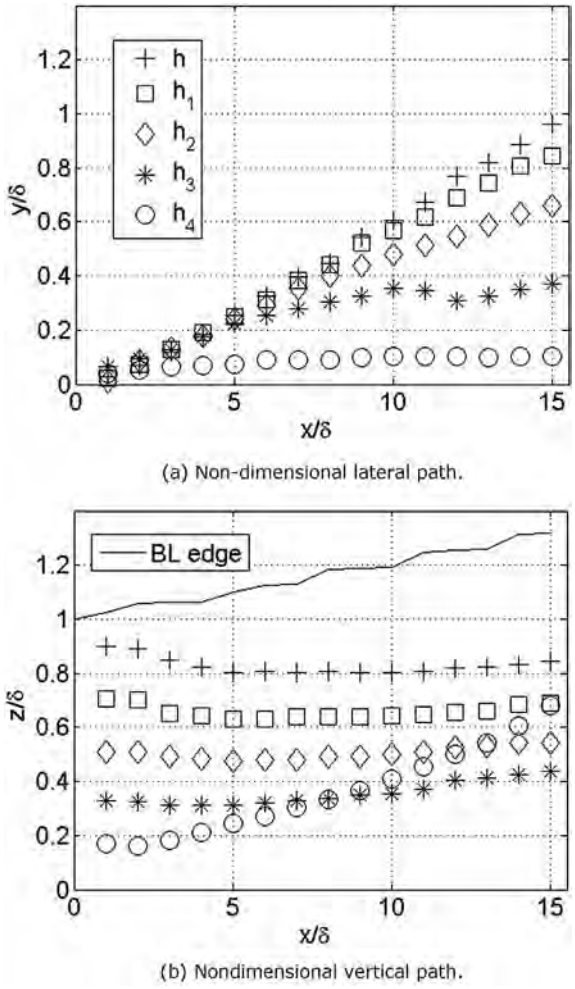

Fig. 7 Influence of VG scaling on vortex core trajectory. Note that the streamwise distance x are normalized by the boundary layer thickness at the VG position d.

Table 1 e VG cases, device heights with respect to the local BL thickness d, drag coefficients, drag decreasing rates and positive circulations at x/d ¼ 5.

VG	*h*/d	C_D	DC_D (%)	$G^þ$ (m^2 s^{-1})
h	1	0.17 86	100	1.20
h_1	0.8	0.15 85	88	0.82
h_2	0.6	0.13	75	0.61

		40		
h_3	0.4	0.10	59	0.43
		54		
h_4	0.2	0.07	44	0.38
		96		

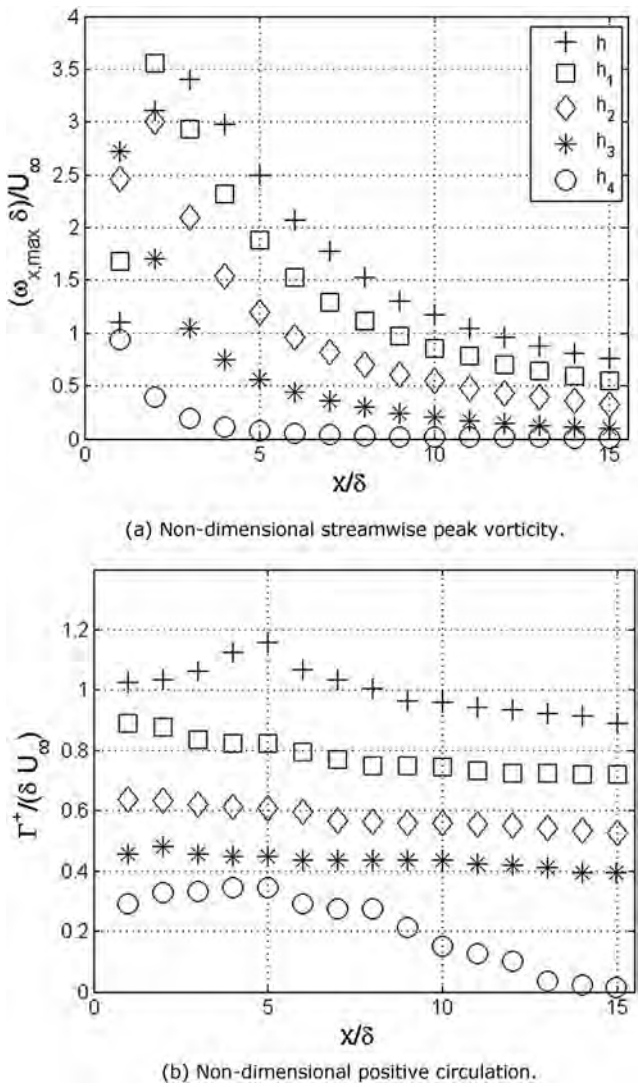

Fig. 8 Influence of VG scaling on vortex decay and vortex strength.

studied cases. For the standard VG case *h*, the largest value of the peak vorticity is achieved straight away behind the vane at the position *x*/d ¼ 3. For the VG cases h_1 and h_2 this maximum value is reached at *x*/d ¼ 1.9 and for the VG case h_3 at *x*/d ¼ 0.9. According to Fig. 8a the vorticity values decreases exponen- tially across the downstream direction *x*/d. The value of the peak vorticity decays as the size of the vane is decreased for all cases. Note that he conventional VG

reaches lower maximum value than the VG case h_1 even though it is higher.

For the visualization of vortical flow structures in 3D tur- bulent fields the Q-criterion scalar has been used. Iso-surface of Q ¼ 0.09 s^{-2} indicating vortex features behind and around the VG is illustrated in Fig. A1 of Appendix A for all the VG cases. The Q-criterion was defined by Q ¼ ½ðkUk^2 – kSk^{2}Þ where U is the spin tensor and S is the strain-rate tensor. The positive value for Q indicates that the flow is vorticity- dominated.

The positive circulation G^{þ} has been determined to esti- mate the strength of the vortex, which is determined by

The non-dimensional positive circulation hardly differs at the downstream plane locations studied for the VG cases h, h_1, h_2, h_3, which is in concordance with the study made by Ashill et al. [21]. For the standard VG h, a slight increasing of the positive circulation is observed in the near wake plane posi- tions and the maximum value is reached at x/d ¼ 5. This peak could be explained because the vortex is not fully developed before the position five times the device height farther downstream of the VG, which is in concordance with [17]. However, the behavior of the VG case h_4 is not in concordance with the other cases. In the case of the lowest VG h_4, the non- dimensional positive circulation development of downstream of the vane differs notably from the other cases and its greatest rate is reached at x/d ¼ 4 plane. Viscosity does not dominate the whole shear layer but only a thin part close to the wall (the so-called near-wall layer) while viscous effects can be safely neglected in the outer layer. In the outer part of the boundary layer, the action of the pressure rise is defined as a direct decrease in the dynamic pressure head along every streamline and the back pressure strength is compensated by the inertia forces. On the other hand, the influence of the fluid inertia in the inner part of the boundary layer is excessively small for this mechanism to be possible. The inertia forces at the walls of the flat plate and VG are zero and thus the pressure forces are balanced by the force of the shear. Within the inner part of the BL, a transition between the fluid at the wall and the fluid of the outer layer appears in which the pressure force is completely compensated by the shear force.

Table 1 shows the corresponding drag coefficient C_D for each VG case. The heights of every vane have been considered with a diminution factor of 20% with respect to the conven- tional VG height h. However, this decreasing rate in the VG height is not followed by the drag coefficients, as indicated in the fourth column of Table 1. The drag decreasing rate DC_D (%) is defined as the relationship between the C_D associated to the low-profile VG h_i and the C_D of the conventional VG height h. The lowest device h_4 with a vane height of 20% of h, has a 44% of the drag of the conventional VG h. The reason could be

found in the fact that as the VG height is decreasing the vane is closer to the BL buffer zone or even to the viscous sublayer, where the viscous shear is dominant.

Table 1 also shows the normalized positive circulation value at plane position $x/d = 5$ in the last column. As expected, that value decreases as the vane height decreases. The con- ventional VG *h* with the largest drag also produces the largest positive circulation and the VG h_4 the lowest circulation with the lowest associated drag as well. Nevertheless, its inferior vortex strength makes this arrangement less efficient than the standard case.

Vortex size

The vortex size is an important and necessary parameter when modelling vortices analytically. The method developed in Ref. [17] uses a parameter ε to define the vortex size as the radial distance from the center of the vortex to the point where the azimuthal velocity u_q achieves the greatest absolute value. Other approaches define the size of the vortex as the radial distance from the vortex center to the point where the axial vorticity u_x decays to zero. However, the use of the mentioned second approach to define the vortex size in flow control and mixing applications can be inconsistent due to the presence of bodies, as the flat plate presented in this study. The interaction of the vortex created by the VG with the plate creates a secondary vortex [13] which makes these two ap- proaches unsuitable for measuring size. With the aim to avoid these inaccuracies, an alternative method is proposed and used in this study to define the size of the vortex based on the vorticity. The axial vorticity u_x distribution of the generated vortex measured in a cross-stream plane tends to be Gaussian but this assumption doesn't fit simulations or experiments at lateral coordinates far away from the center of the vortex. For this reason, the introduction of the half-life radius concept $R_{0.5}$ is desirable, which is a more accurate method to define the vortex size.

The half-life radius defines the distance from the center of the vortex to the point where the vorticity is half of the peak vorticity measured in a cross-stream plane. At that point, the errors when estimating the vortex radius are now insignifi- cant for both computational and experimental data and, consequently, the degree of accuracy can be improved. A vi- sual representation of $R_{0.5}$ can be observed in Fig. 9, where a set of data corresponding to the vorticity distribution induced by the conventional VG case *h* in a plane located at $x = 5d$ is plotted and fitted to a Gaussian distribution. Thus, the vorticity in a plane normal to the flow can be described by the radial coordinate *r*, the half-life radius $R_{0.5}$ and the local peak vorticity u_{peak} according to Equation (3).

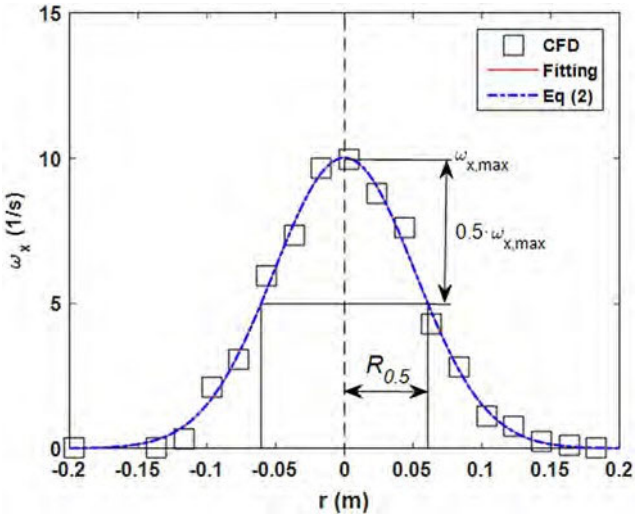

Fig. 9 Comparison between the axial vorticity through the center of the vortex core and a Gaussian distribution of similar shape defined in Equation (3). CFD data extracted for the conventional VG h at the cross-plane position 5d downstream of the VG.

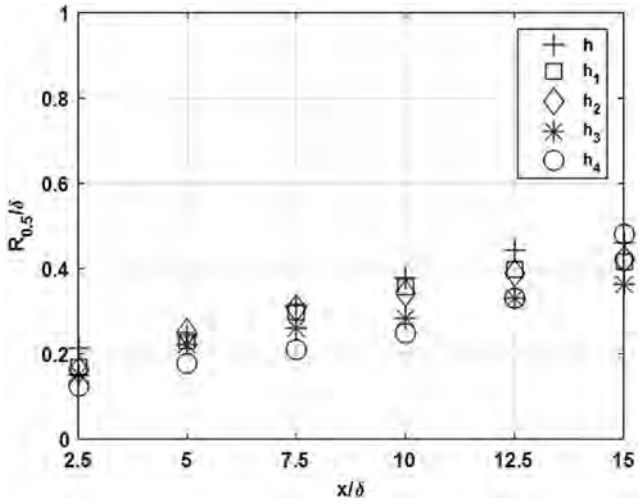

Fig. 10 e Vortex size evolution expressed in terms of the half-life radius at different streamwise distances for all the VG cases.

ize of the primary vortex is similar to the one generated by the so-called conventional VG with height the local BL thick-The half-life radius has been extracted for all the VG cases and plane positions from 2.5d to 15d measured downstream of the VG trailing edge. Fig. 10 shows the vortex size evolution for all VG cases at different locations downstream of the device and normalized by the local BL thickness d. These results tend to increase in a linear way when moving downstream for each ness h ¼ d. The size of the vortex generated by the lowest VG h_4 increases farther downstream of the vane and it is even larger than the vortex size corresponding

to the conventional VG *h* at the plane position x/d ¼ 15. At that position, the vortex generated by the lowest VG h_4 is almost dissipated and a sig- nificant uncertainty in defining the vortical structure that determines the vortex radius was found.

A prediction model might be a desirable tool as a flexible approach to estimate the primary vortex size generated by different VGs. Controlling of near-wall longitudinal vortices has a huge applicability in the engineering field since these generated vortices can transfer both heat and momentum from the outer part of the boundary layer to the inner part, re- energizing the lowest part of the boundary layer. Therefore, to be able to control and optimize parameters such the size of the vortex to the flow setting is greatly desired. Consequently, the development of new models which can reproduce the vortex behavior is of high interest. This ideal tool would predict the vortex size based on the geometric properties of the device (e.g. the VG height) and the flow properties in which it is placed (e.g. the local boundary layer thickness). Taking into account the linear evolution of the vortex half-life radius shown in Fig. 10 along the streamwise direction and the VG cases considered, the values obtained for the vortex half radius are fitted to a surface as a fairly good attempt to empirically describe the behavior of the vortex size. As a result, a linear polynomial-type surface fitting the CFD results may be generated like the one shown in Fig. 11 and conse- quently, the mathematical expression corresponding to this surface which defines the non-dimensional vortex size may be the following one:

$$\frac{R0{:}5}{d} \text{¼} A \text{þ} B\$ \frac{h}{d} \text{þ} C\$ \frac{x}{} \qquad (4)$$

was found as 0.008052. This expression obtained for vane-type vortex generators would eventually allow estimating the vortex size for any single vortex generator which complies with the Reynolds number *Re* and the vane incident angle in the present work.

The prediction model presented in Equation (4) fits rela- tively well the computational results for all the VG cases even for the downstream plane position 2.5d behind the VG where the primary vortex seems to be not fully developed as shown in Velte et al. [13]. However, in the most unfavorable situation which is the lowest VG h_4 at the farthest plane position 15d, the deviations between the vortex half-life radius estimated by this analytical model and the simulated half-life radius are relatively meaningful, probably due to the difficulty on finding the vortex core center because the vortex is almost dissipated at that distance downstream of the VG. Notice that the results regarding the VG h_4 are in concordance with the preliminary conclusions explained in Section Trajectory of the streamwise vortex and Vortex decay where the VG h_4 also had a different behavior when comparing with the results obtained for the rest of the cases. The lowest vane generates a longitudinal vortex near to the plate wall and as a

result, a great interaction with the wall was originated.

Figs. B1 and B2 of Appendix B display the vortices by con- tours of the streamwise velocity for all the VG cases at several plane positions downstream of the devices and show a qual where the coefficients A, B and C are 0.05639, 0.1055, and 0.02023 respectively for the set of non-dimensional VG heights *h*/d and streamwise distances *x*/d computed on a 95% confi- dence interval. The 95% confidence intervals for these three coefficients are [0.02426, 0.08853], [0.06906, 0.142] and [0.01781, 0.02264] respectively. The correlation coefficient value was determined as 0.9774 and the root mean square error (RMSE)

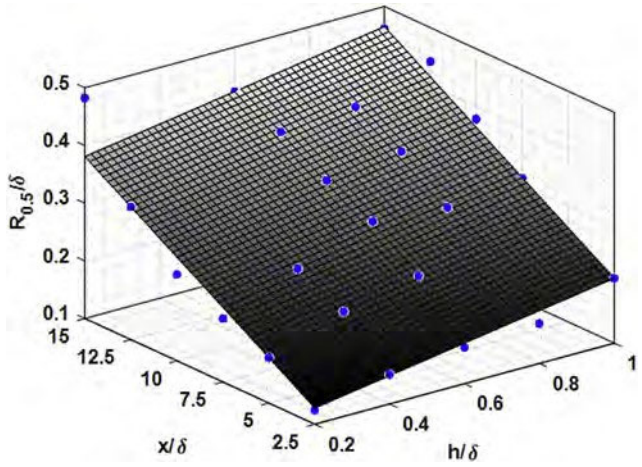

Fig. 11 The non-dimensional vortex half-life radius represented by blue dots ( ) as a function of the non- dimensional VG height h/d and the streamwise distances x/d and its corresponding polynomial-type surface fitting. (For interpretation of the references to colour in this figure legend, the reader is referred to the web version of this article.)

cases *h*, h_1 and h_2, the primary vortex is clearly defined and identifiable. According to Fig. B1, the largest vortex size is produced by the conventional VG case *h* ¼ d, which is in agreement with the results shown in Fig. 10. The contours of the vortices of the lowest VG case h_4 have not been presented in Appendix B because the vortex contours were not displayed at the scale used for comparison.

Conclusions

In the current work, the primary vortex that is generated by a vane type vortex generator with

rectangular shape has been investigated in order to provide a better understanding of the main characteristics of the primary vortex downstream of the vortex generator. Five different heights equal or lower than the boundary layer thickness at the VG position have been investigated, h ¼ d, h_1 ¼ 0.8d, h_2 ¼ 0.6d, h_3 ¼ 0.4d and h_4 ¼ 0.2d. These low profile vortex generators have proven to be a sim- ple, cheap and low drag solution to flow control applications. Numerical computations of these passive devices within a turbulent boundary layer flow over a flat plate with a negli- gible streamwise pressure gradient have been conducted. The Reynolds number is Re_d ¼ 1350, based on the boundary layer thickness at the VG position d ¼ 0.25 m.

Both path and non-dimensional peak vorticity of the vortex generated downstream of the VG are significantly affected by its height. The trajectories followed by the vortex produced by low profile VGs h_1, h_2 and h_3 the same trend of the conven- tional VG height. Nevertheless, the VG case h_4 is different for both lateral and vertical directions in comparison with the conventional VG h and the other low-profile devices h_1, h_2, h_3. One explanation for this different behavior could be found in

the fact that the vortex generated by the VG case h_4 creates a vortex whose path is different for both vertical and lateral directions when compared with the conventional and the other low profile devices. One explanation for this behavior could be found in the closeness of the vortex generated by the low profile VG case h_4 to the wall, and the interference with the inner side of the boundary layer, where viscous shear stress and its interaction with the wall is dominant. For all the studied cases, the conventional height VG with the major drag produces the largest positive circulation, while the case h_4 produces the lowest circulation and the lowest associated drag as well.

Additionally, a prediction model based on two elementary parameters as the non-dimensional VG height and the non- dimensional downstream position has been developed. This model consists of a linear polynomial-type surface which fits relatively well the computational results. The model is able to describe the vortex size evolution in a simple way with no limitations on the shape of the vortex core center. This new approach is a key issue for a fundamental understanding of the VGs and it could eventually help in the design of real VG

applications (e.g. wind turbine blades or aircraft wings) where certain parametric studies can be considerably reduced in terms of time and cost by facilitating engineering tools.

Acknowledgements

The authors are grateful to European Union Ministry of Turkey, National Agency of Turkey for the support of this project under the Project Code: 2015-1-TR01-KA203-021342 entitled Innovative European Studies on Renewable Energy Systems. Technical and human support provided by IZO-SGI, SGIker (UPV/EHU, MICINN, GV/EJ, ERDF and ESF) is gratefully acknowledged. Computations were made using of ARINA PC- cluster at UPV/EHU. The authors also wish to acknowledge CD-Adapco for providing the CFD solver.

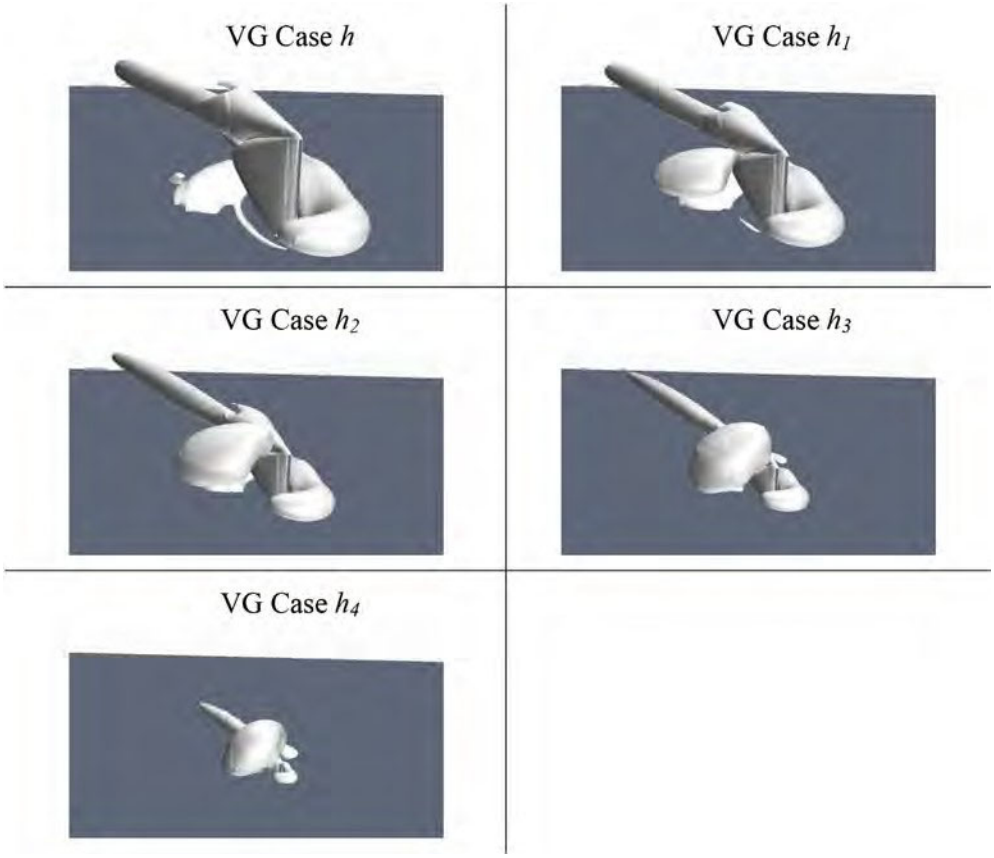

Fig. A1: 3D vortical flow structures visualized by Q scalar for all the VG cases.

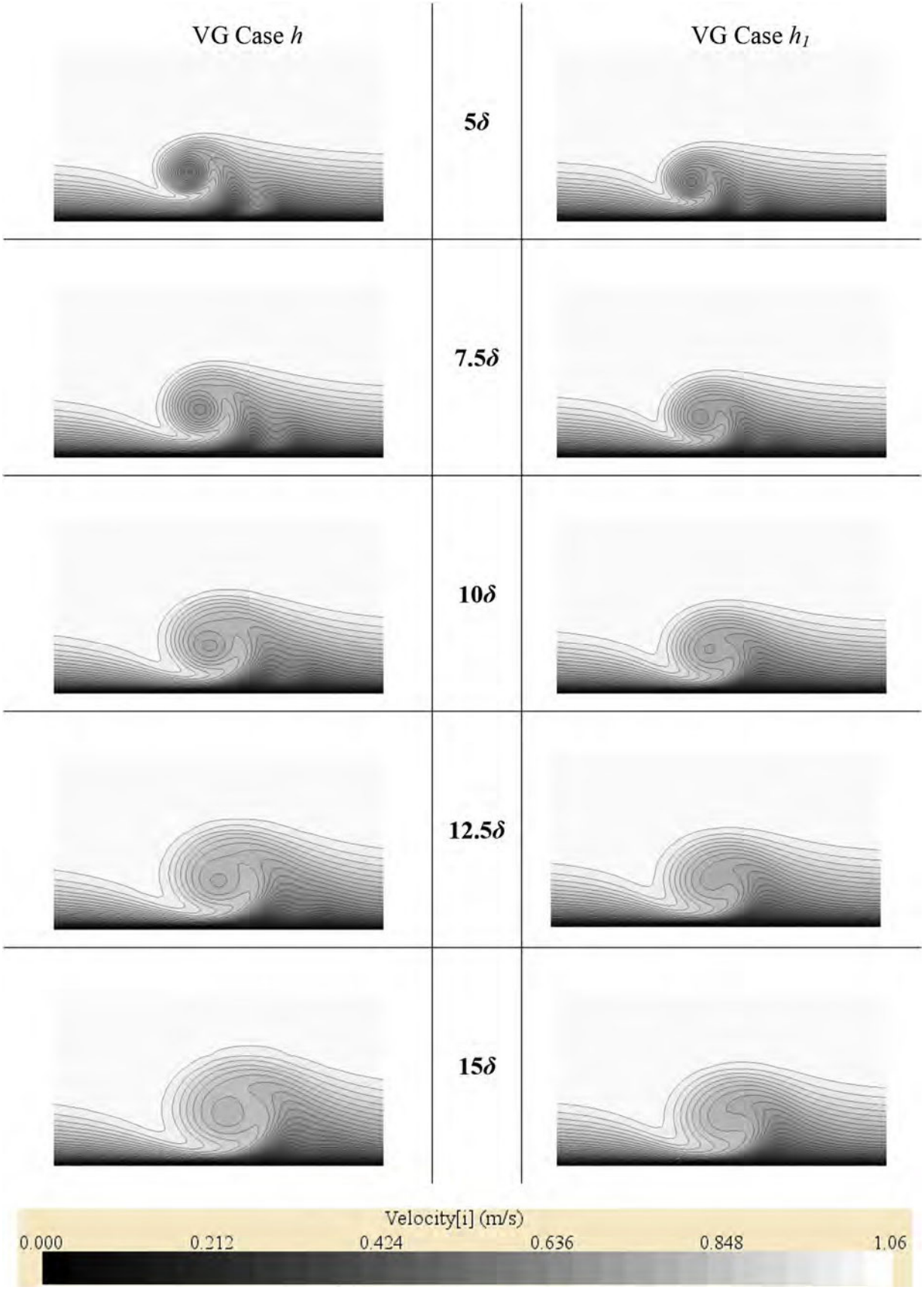
VG Case h
VG Case h_1
5δ
7.5δ
10δ
12.5δ
15δ
Velocity[i] (m/s)
0.000
0.212
0.424
0.636
0.848
1.06

Fig. B1: Downstream development of the device wake for the VG cases h (left column) and h_1 (right column). The vortices are displayed by axial velocity contours u_x at five plane position 5d, 7.5d, 10d, 12.5d and 15d downward.

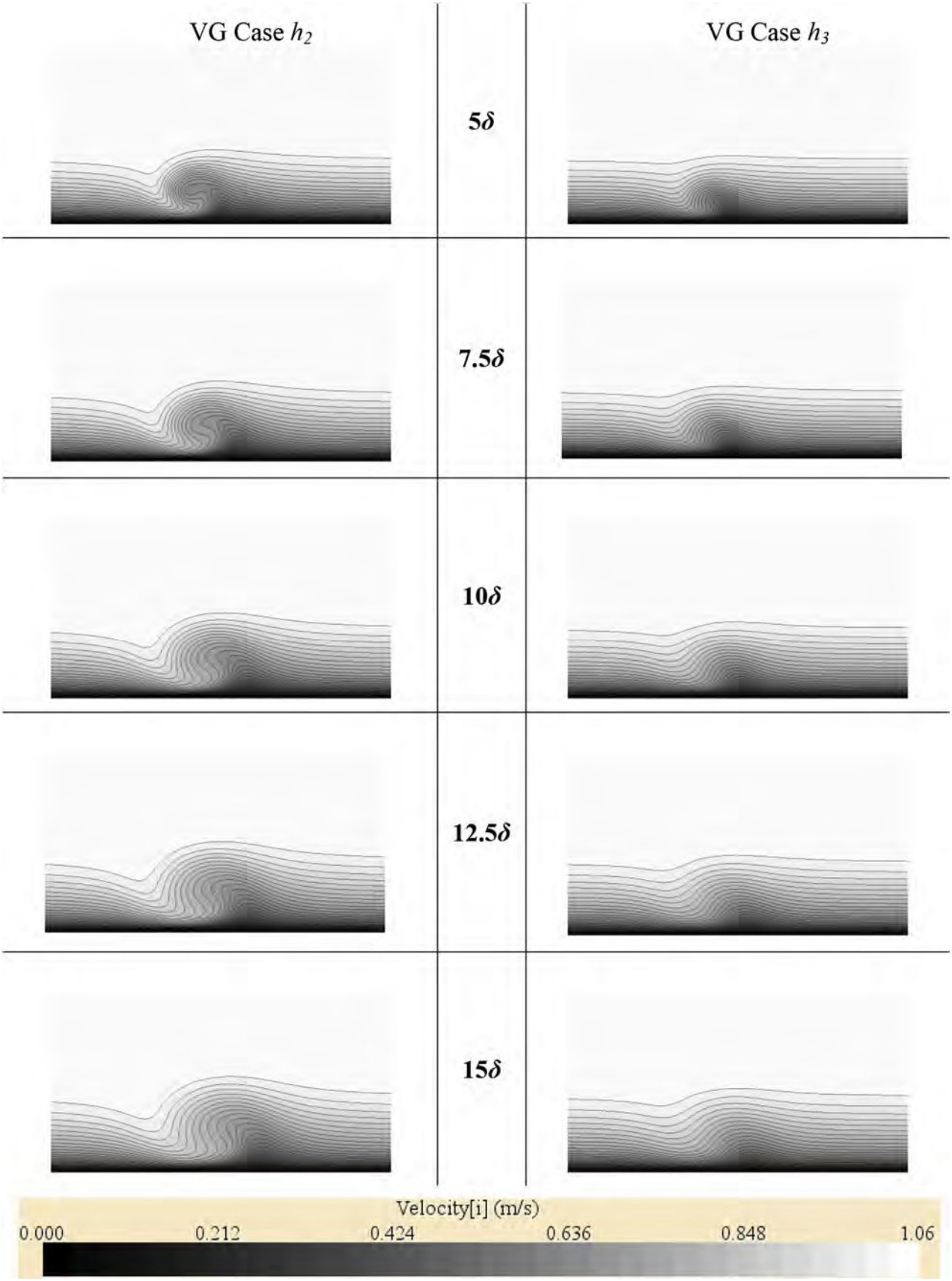

Fig. B2: Downstream development of the device wake for the VG cases h_2 (left column)

and h_3 (right column). The vortices are displayed by axial velocity contours u_x at five plane position 5d, 7.5d, 10d, 12.5d and 15d downward.

1) Ç akir MT. The wind energy potential in Turkey and its position among EU countries. Politeknik Derg 2010;13(4).
2) Dai H, Silva Herran D, Fujimori S, Masui T. Key factors affecting long-term penetration of global onshore wind energy integrating top-down and bottom-up approaches. Renew Energy 2016;85:19e30. http://dx.doi.org/10.1016/ j.renene.2015.05.060.
3) Espan~a G, Aubrun S, Loyer S, Devinant P. Wind tunnel study of the wake meandering downstream of a modelled wind turbine as an effect of large scale turbulent eddies. J Wind Eng Ind Aerodyn 2012;101:24e33. http://dx.doi.org/10.1016/ j.jweia.2011.10.011.
4) Kim S, Shin H, Joo Y, Kim K. A study of the wake effects on the wind characteristics and fatigue loads for the turbines in a wind farm. Renew Energy 2015;74:536e43. http:// dx.doi.org/10.1016/j.renene.2014.08.054.
5) Kahla S, Soufi Y, Sedraoui M, Bechouat M. On-off control based particle swarm optimization for maximum power point tracking of wind turbine equipped by DFIG connected to the grid with energy storage. Int J Hydrogen Energy 2015;40(39):13749e58. http://dx.doi.org/10.1016/ j.ijhydene.2015.05.007.
6) Dahbi A, Nait-Said N, Nait-Said M. A novel combined MPPT- pitch angle control for wide range variable speed wind turbine based on neural network. Int J Hydrogen Energy 2016;41(22):9427e42. http://dx.doi.org/10.1016/ j.ijhydene.2016.03.105.
7) Becker R, Garwon M, Gutknecht C, Ba€rwolff G, King R. Robust control of separated shear flows in simulation and experiment. J Process Control 2005;15(6):691e700. http:// dx.doi.org/10.1016/j.jprocont.2004.12.001.
8) Wang Y, Li S, Yang X, Deng Y, Su C. Numerical and experimental investigation for heat transfer enhancement by dimpled surface heat exchanger in thermoelectric generator. J Electron Mater 2016;45(3):1792e802. http:// dx.doi.org/10.1007/s11664-015-4228-0. Available: http://dx. doi.org/10.1007/s11664-015-4228-0.
9) Gao L, Zhang H, Liu Y, Han S. Effects of vortex generators on a blunt trailing-edge airfoil for wind turbines. Renew Energy 2015;76:303e11. http://dx.doi.org/10.1016/ j.renene.2014.11.043.
10) Choudhry A, Arjomandi M, Kelso R. Methods to control dynamic stall for wind turbine applications. Renew Energy 2016;86:26e37. http://dx.doi.org/10.1016/

j.renene.2015.07.097.
11) Gebhardt CG, Preidikman S, Massa JC. Numerical simulations of the aerodynamic behavior of large horizontal-axis wind turbines. Int J Hydrogen Energy 2010;35(11):6005e11. http:// dx.doi.org/10.1016/j.ijhydene.2009.12.089.
12) Smith FT. Theoretical prediction and design for vortex generators in turbulent boundary-layers. J Fluid Mech 1994;270:91e131. http://dx.doi.org/10.1017/ S0022112094004210.
13) Velte CM, Hansen MOL, Okulov VL. Helical structure of longitudinal vortices embedded in turbulent wall-bounded flow. J Fluid Mech 2009;619:167e77. http://dx.doi.org/10.1017/ S0022112008004588.
14) for navier-stokes codes. In: Presented at proceedings of the 1999 3rd ASME/JSME joint fluids engineering conference, FEDSM'99; 1999.
15) Fernandez-Gamiz U, Re'thore' P, Sørensen NN, Velte CM, Zahle F, Egusquiza E. Comparison of four different models of vortex generators. In: Presented at proceedings of EWEA 2012-European wind energy conference & exhibition; 2012.
16) Schubauer GB, Spangenberg WG. Forced mixing in boundary layers. J Fluid Mech 1960;8(1):10e32. http://dx.doi.org/ 10.1017/S0022112060000372.
17) Velte CM. Vortex generator flow model based on self- similarity. AIAA J 2013;51(2):526e9. http://dx.doi.org/10.2514/ 1.J051865.
18) Fernandez-Gamiz U, Velte CM, Re'thore' P, Sørensen NN, Egusquiza E. Testing of self-similarity and helical symmetry in vortex generator flow simulations. Wind Energy 2016;19(6):1043e52. http://dx.doi.org/10.1002/we.1882.
19) Lin JC, Howard FG, Selby GV. Small submerged vortex generators for turbulent-flow separation control. J Spacecr Rockets 1990;27(5):503e7.
20) Yao CS, Lin JC, Allan BG. Flowfield measurement of device- induced embedded streamwise vortex on a flat plate. In: Presented at 1st flow control conference, fluid dynamics and co-located conferences; 2002. http://dx.doi.org/10.2514/ 6.2002-3162.
21) Ashill P, Fulker J, Hackett K. Research at DERA on sub boundary layer vortex generators (SBVGs). In: Presented at 39th AIAA aerospace sciences meeting and exhibit, AIAA paper 2001-0887; 2001.
22) Lin JC. Review of research on low-profile vortex generators to control boundary-layer separation. Prog Aerosp Sci 2002;38(4e5):389e402. http://dx.doi.org/10.1016/S0376-0421(02)00010-6.
23) Khosla PK, Rubin SG. A diagonally dominant second-order accurate implicit scheme. Comput Fluids 1974;2(2):207e9. http://dx.doi.org/10.1016/0045-7930(74)90014-0.
24) Menter FR. Two-equation eddy-viscosity turbulence models for engineering applications.

AIAA J 1994;32(8):1598e605. http://dx.doi.org/10.2514/3.12149. Available: http://dx.doi.org/10.2514/3.12149.

25) Allan BG, Yao C, Lin JC. Numerical simulations of vortex generator vanes and jets on a flat plate. In: Presented at 1st flow control conference. Fluid dynamics and co-located conferences; 2002. http://dx.doi.org/10.2514/6.2002-3160.

26) Stanislas M, Godard G. Control of a decelerating boundary layer. part 1: optimization of passive vortex generators. Aerosp Sci Technol 2006;10(3):181e91. http://dx.doi.org/10.1016/j.ast.2005.11.007.

27) Vinokour M. On one-dimensional stretching functions for finite-difference calculations. J Comput Phys 1983;50(2):215e34. http://dx.doi.org/10.1016/0021-9991(83) 90065-7.

28) Batchelor GK. Axial flow in trailing line vortices. J Fluid Mech 1964;20(4):645e58. http://dx.doi.org/10.1017/ S0022112064001446.

29) Pearcey HH. Introduction to shock-induced separation and its prevention by design and boundary layer control. In: Boundary layer and flow control; 1961. http://dx.doi.org/10.1016/B978-1-4832-1323-1.50021-X.